Front. Phys. 12(6), 120505 (2017)
DOI 10.1007/s11467-017-0658-x

RESEARCH ARTICLE

Detectable states, cycle fluxes, and motility scaling of molecular motor kinesin: An integrative kinetic graph theory analysis

Jie Ren

Center for Phononics and Thermal Energy Science, School of Physics Science and Engineering, Tongji University, 200092 Shanghai, China
Corresponding author. Email: xonics@tongji.edu.cn
Received November 3, 2016; accepted December 22, 2016

The process by which a kinesin motor couples its ATPase activity with concerted mechanical hand-over-hand steps is a foremost topic of molecular motor physics. Two major routes toward elucidating kinesin mechanisms are the motility performance characterization of velocity and run length, and single-molecular state detection experiments. However, these two sets of experimental approaches are largely uncoupled to date. Here, we introduce an integrative motility state analysis based on a theorized kinetic graph theory for kinesin, which, on one hand, is validated by a wealth of accumulated motility data, and, on the other hand, allows for rigorous quantification of state occurrences and chemomechanical cycling probabilities. An interesting linear scaling for kinesin motility performance across species is discussed as well. An integrative kinetic graph theory analysis provides a powerful tool to bridge motility and state characterization experiments, so as to forge a unified effort for the elucidation of the working mechanisms of molecular motors.

Keywords graph theory, molecular motor, state detection, cycle flux, motility scaling

PACS numbers 05.40.-a, 05.60.Cd

1 Introduction

Conventional kinesin [1–3] is the original member of a large and still growing superfamily of cytoskeleton-based motor proteins, and serves as an archetypical model system for molecular motor study. Conventional kinesin is a homodimer made of two globular motor domains (often called heads) that can each bind a microtubule (MT) track and catalyze ATP hydrolysis. The dimer as a whole can make hundreds of consecutive ∼8.2-nm steps in a hand-over-hand fashion and maintain sturdy direction toward the MT plus end against loads of several pN. Kinesin's concerted steps and high processivity imply coordination or "gating" between its two motor domains.

Previous experiments found evidence for two types of gatings that presumably keep the catalytic cycles of the two motor domains out of phase: when kinesin is bound to MT by two heads, ATP binding to the front head is prohibited [4–6], and ADP release from the rear head is severely retarded [7–9]. The experimental identification and chemical/mechanical characterization of major dimer-MT states occurring in kinesin's steps present a major route towards the elucidation of kinesin's chemomechanical mechanisms. While measured states of truncated monomers on MT suggest a large number of possible dimer-MT states, only a subset of these states actually occurs and plays a functional role in kinesin's steps as a consequence of gating effects. The subset of functionally relevant dimer-MT states, together with transition patterns in conformity with the chemomechanical coupling, forms kinesin's basic kinetic landscape. To map out this dimer-level kinetic landscape is a major focus of kinesin study.

At present, direct experimental characterization of intermediate dimer-MT states, particularly at the single-molecule level, remains difficult, and has seen only modest success [10–13]. However, single-molecule measure-

*Special Topic: Soft-Matter Physics and Complex Systems (Ed. Zhi-Gang Zheng).

ment of kinesin's overall performance was achieved a decade ago and has accumulated a large body of high-precision data on velocity [12, 14–16] and consecutive run length [17–21]. Though kinesin's motility performance and state occurrence are both dictated by the same underlying kinetic graph, the existing wealth of motility data has little direct bearing on the state characterization effort to date. To bridge the gap, we present here a theorized kinetic graph that on the one hand is validated by the motility data, and on the other hand allows for the mathematically rigorous quantification of the detectability of states and chemomechanical cycles during kinesin's steps. We shall demonstrate that this integrative kinetic-graph analysis of motility and state characterization experiments provides a new and fertile ground for the elucidation of kinesin's working mechanisms.

2 Results

2.1 Proposed kinetic graph

The kinetic graph consists of three single-headed and four two-headed kinesin-MT binding states together with 10 pairs of transitions between these basic states (Fig. 1). Single-molecule measurements found direct evidence of the existence of a two-headed state S1 (and S2 thereby inferred) [10–12, 22], and a one-headed state S3 (and S4, 5, and 6 thereby inferred) [12, 13, 23]. A recent mechanical measurement [24] reported purely load-induced consecutive steps in an nucleotide-free buffer, implying the existence of a nucleotide-free state S7. Moreover, previous mechanical calculations [25–27] suggested that two-headed states S1, S2, and S7 are thermodynamically stable compared with single-headed configurations. The ATP gating was implemented in the kinetic graph by excluding all transitions that involve ATP binding to the front head in two-headed kinesin-MT states. In two-headed kinesin-MT binding states, the intramolecular force was estimated [27, 28] to be above 12 pN. This rear-pointing force upon the front head greatly amplifies its ATP dissociation rate, effectively guaranteeing the ATP gating.

The ADP gating mainly affects the backward diffusive attachment of the ADP-bound head. The forward-pointing force prohibits the release of ADP from the rear head, which makes the ADP retaining two-headed state a transient state, as implied by recent experiments [12, 13]. This is consistent with the finding [29] that the head-MT binding affinity is ∼12.5 kJ/mol lower for the ADP state than for the ATP or nucleotide-free state. In addition, mechanical computations [27] confirmed that the ADP-retaining two-headed state is thermodynamically unstable because it has a total free energy comparable to that of the single-headed state (e.g., S3, S4). Therefore, the kinetic graph neglected this transient state, and only allowed forward diffusive attachment of an ADP-bound head (i.e., transitions S3 → S7). For the forward attachment of an ADP-bound head (e.g., S3 → S7, S4 → S1, and S5 → S2), instantaneous ADP release was assumed.

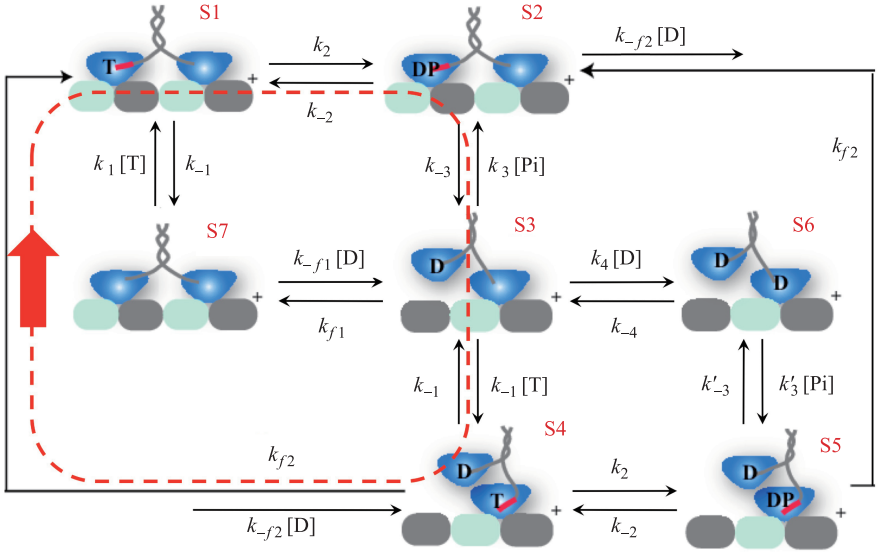

Fig. 1 Kinesin's fundamental kinetic landscape proposed in this study. Illustration of kinesin-MT interaction states (marked by S1–S7), and transitions (*arrows*) among them. In the state illustrations, T, D, P, DP mark ATP, ADP, Pi and ADP·Pi respectively. The bold line (*red*) indicates the neck linker in an ATP-induced zipper state. The dashed line (*red*) marked by the big arrow (*red*) indicates kinesin's main chemomechanical cycle for normal walking.

The kinetic graph (namely, its states and transition rates) dictates state occurrence, chemomechanical cycling, and motility performance. Any recurring step of kinesin corresponds to a self-closed cycle of dimer-MT states. In this study, we apply the graph theory to exhaustively enumerate all possible chemomechanical cycles allowed by the kinetic graph, and compute a completion frequency for each cycle and an occurring probability for each state. Because the state occurring probability and cycle completion frequency (i.e., cycle flux) are proportional to the chance by which the state and cycle can be detected during kinesin's steps, we were able to rank the detectability of the states and cycles in a mathematically rigorous way. This allowed us to identify kinesin's major intermediate states and dominant chemomechanical cycles, in order to predict the motility performance. The validity of the proposed kinetic graph is confirmed by confronting its predictions with kinesin's comprehensive phenomenology established by previous motility and state detection experiments.

2.2 Graph theory methods for calculating kinetics

Velocity and run length. The kinetic network proposed for kinesin (Fig. 1) is represented by a graph that contains seven vertices (i.e., states) and 10 pairs of edges (i.e., transitions linking two neighboring vertices). A cycle C is defined as a self-closed series of states through which kinesin hops in the kinetic landscape by means of consecutive chemomechanical transitions. The velocity is obtained by summing over all cycles that cause a backward or forward step, namely, $\langle v\rangle = L_0\sum_C(J_{C+}-J_{C-})(L_0 = 8.2\ \text{nm})$ [30]. The mean run length is $\langle L\rangle = \langle v\rangle/\sum_i p_i^s\gamma_i$ [30]. The summation is over single-headed kinesin-MT binding states, and γ_i is the derailment rate. We exhaustively enumerate all cycles for kinesin's kinetic graph using a depth-first algorithm (detailed in Methods). The frequency for cycle completion (or cycle flux) $J_{C\pm}$ is computed using an algebraic formula, which is derived in this study as follows. The state occurring probability p_i^s in $\langle L\rangle$ is obtained from steady-state solutions of the master equation in terms of the proposed kinetic graph.

Steady-state probability calculation of states. The master equation in terms of the seven dimer-MT states contained in the proposed kinetic graph for kinesin (Fig. 1) is $\dot{\boldsymbol{p}}(t) = -W\boldsymbol{p}(t)$. Here, $\boldsymbol{p} = \{p_1, \cdots, p_N\}$ $(N = 7)$ denote the occupation probabilities of these states at time t and that satisfy probability conservation. W is the transition matrix or Laplacian $W_{ij} = -\omega_{ij} + \delta_{ij}\sum_m \omega_{mj}$, where ω_{ij} denotes the rate of transition from the jth to ith state. For example, in Fig. 1, $\omega_{17} = k_1\cdot[\text{ATP}]$, $\omega_{71} = k_{-1}$. The transition rates used in this study are listed in Table 1. Using Cramer's rule, the steady-state solution can be easily obtained as $p_i^s = \frac{\det(W[i;i])}{\sum_i \det(W[i;i])}$. Here, $\det(W[j;i])$ is the determinant of the matrix $W[j;i]$ that results from deleting row j and column i of W.

Steady-state flux calculation of cycles. The frequency of cycle completions (cycle flux) was formulated by the graph theory [35–37] as $J_{C\pm}^s = \Sigma_C\Pi_{C\pm}/\Sigma$, where C_+ and C_- denote the forward and backward one-way cycles, $\Pi_{C\pm}$ is the weight of the one-way cycle, Σ_C is the sum of weights of spanning trees that are rooted on cycle C, and Σ is the sum of weights of spanning trees rooted on all states. The weight of a subgraph is defined as the product of the transition rates forming it. In practice, it is difficult to count the spanning trees rooted on all of the vertices. We surmounted this problem by deriving simple algebraic expressions for the cycle fluxes using algebraic graph theory.

The generalized matrix-tree theorem [38] states that the principal minor of Laplacian W of a weighted graph G, obtained by deleting row i and column i of W, has determinant $\det(W[i;i])$, which is equal to the sum of weights of directed spanning trees wherein every link is oriented towards vertex i (rooted at i). Namely, $\det(W[i;i]) = \Sigma_i$. The steady-state probabilities may then be rewritten as $p_i^s = \Sigma_i/\Sigma$, in which $\Sigma = \sum_i \det(W[i;i])$. This algebraic expression has an intuitive interpretation in terms of graphs [39] because the flow of directed links towards a state is associated with transition rates that lead towards the state and increase its chance of occupation. Σ_C also has a simple algebraic expression. Notice that the sum of weights of spanning trees rooted on cycle C in graph G is identical to the sum of weights of directed spanning trees rooted at a vertex d in the new graph G'' that is obtained by shrinking cycle C into a single vertex d. The above statement can be expressed algebraically as $\Sigma_C = \Sigma_d'' = \det(W''[d;d])$. $W''[d;d]$ results from deleting row d and column d of the new Laplacian matrix corresponding to G''. Further, it is noted that the shrinking operation satisfies the identity $\det(W''[d;d]) = \det(W[C;C])$, where $W[C;C]$ is the matrix that results from deleting rows $i \in C$ and columns $i \in C$ of the original Laplacian matrix W. Thus, $\Sigma_C = \det(W[C;C])$. Finally, we obtain the algebraic expression of the one-way cycle flux:

$$J_{C\pm}^s = \Pi_{C\pm}\frac{\det(W[C;C])}{\sum_i \det(W[i;i])}. \tag{1}$$

2.3 Comparison with motility data

Our comparison focuses on two aspects of motility performance for which high-resolution data are available, namely, average velocity and mean consecutive run length. The comparison is conducted from near-zero to saturating ATP concentrations (≥ 1 mM) [Figs. 2(a, b)]

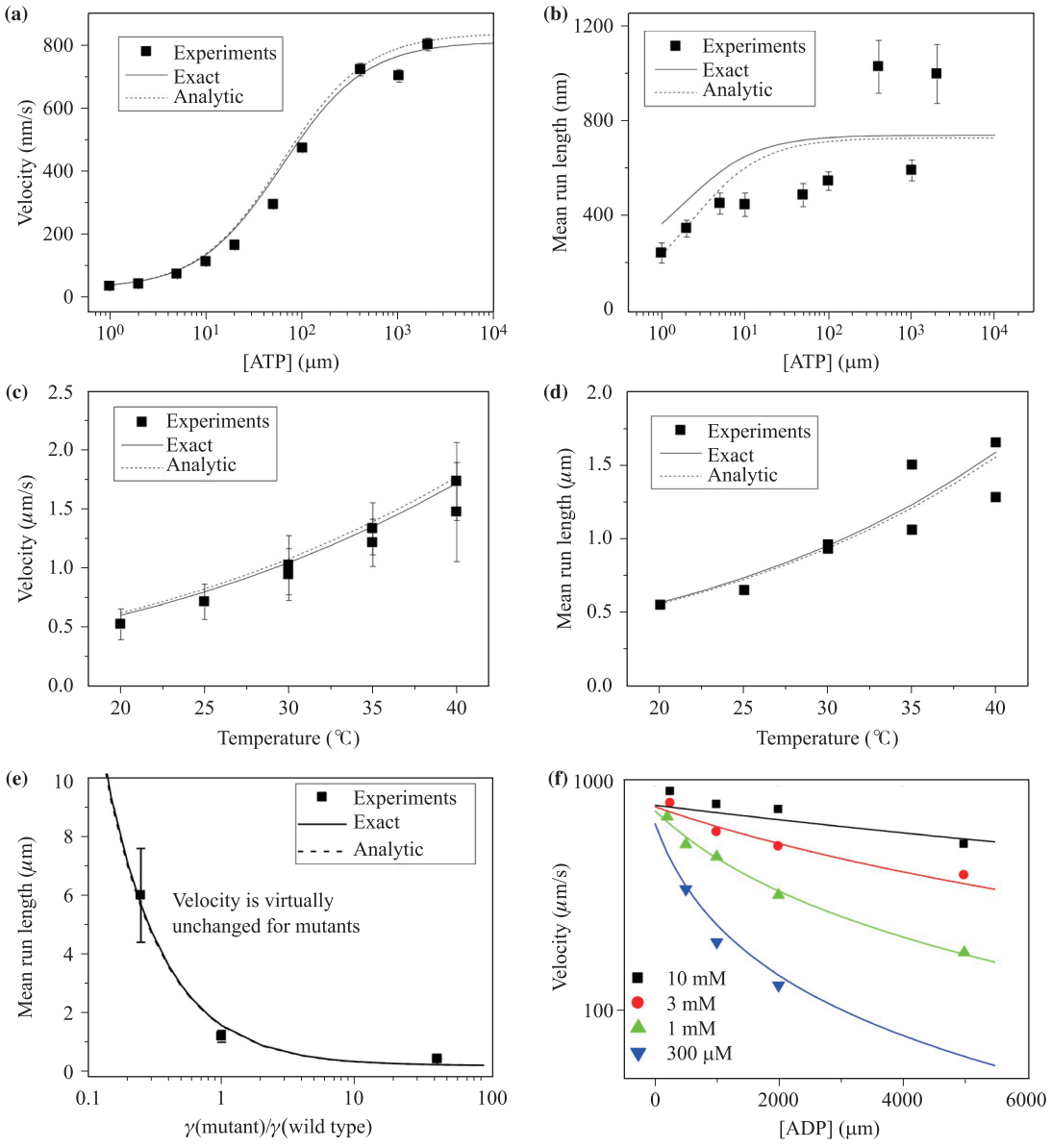

Fig. 2 Comparison to motility experiments for ATP dependence **(a, b)**, temperature dependence **(c, d)**, engineered mutants **(e)**, and ADP dependence **(f)**. Symbols show experimental data. Solid lines are exact predictions by the kinetic landscape sketched in Fig. 1. The dashed lines are predictions from an approximate analytical equation (see Methods). **(a, b)** The experimental data were for squid kinesin under near zero load, room temperature condition, and were taken from Refs. [17, 40]. **(c, d)** The data were for bovine brain kinesin from Refs. [20, 21] with load-free condition and [ATP] = 1 mM. **(e)** The mutants shown in possess modified charged residues in the neck region, which affected mainly the rates for derailment from single-headed binding with MT. The derailment rate ratio between mutants and wild type was obtained by assuming an exponential dependence of the rate on the number of charges in the neck region. The engineered kinesins have almost the same velocity as the wild type kinesin but different run lengths. **(f)** ADP concentration dependence of velocity under different [ATP]. The data were from Ref. [15]. The rates used for all the predictions were listed in Table 1 and Methods.

with a load-free regime. Comparisons are also made for buffer temperatures ranging between 20–40 °C [Figs. 2(c, d)], and for engineered mutations and ADP dependence [Figs. 2(e, f)]. These comparisons yield a theory-experiment agreement that is systematic and satisfactory overall.

For this functionally relevant load-free regime, the kinetic-graph analysis yields a set of analytical formulae for velocity and run length in terms of measurable rates (see Methods). The formulae agree fairly well with the

exact numerical predictions and the experimental data [Figs. 2(a–f)]. This formal agreement provides a consistency check for the proposed kinetic graph.

2.4 Comparison with state characterization data

The kinetic graph allows us to predict the occurring probability for dimer-MT states during kinesin's steps, which roughly corresponds to the state's detectability in experiments. A recent state detection experiment [12] under a zero load found that kinesin spends most of its time with both heads bound to MT during steps at saturating ATP concentrations (1 mM), but stays mostly in a single-headed binding state at low concentrations (a few μM). These features for load-free kinesin are correctly reproduced by this study. The ranked state detectability shows that a single-headed state S3, in which the MT-bound head is nucleotide free and the mobile head binds ADP, is the most probable state from a few μM to 50 μM [Fig. 3(a)]. This is because the lifetime of S3 is determined by a competition between ATP binding to the MT-bound head and the low-rate MT attachment events of the diffusing head before the ATP binding. When ATP binding becomes rate-limiting at low concentrations, kinesin is trapped in S3 with an elongated lifetime. When ATP concentration is raised beyond 500 μM, two-headed states S1 and S2 become the most probable states in which the rear head binds ATP or ADP·Pi.

At the saturating concentration regime, ATP binding to the MT-bound head occurs swiftly to cause a conformational change of the short peptide, which links the motor domain to the coiled-coil dimerization domain (so-called "neck linker zippering") [41]. The zippered neck linker provides a bias by which the diffusing head attaches MT toward the plus end at an amplified rate ($k_{f2} \sim 600\ s^{-1}$) [27]. This leads to two-headed states S1 and S2, the lifetimes of which are determined by hydrolysis and Pi release, respectively. Since hydrolysis is the rate-limiting process at saturated ATP concentrations, S1 dominates kinesin's steps. However, when ATP concentration is extremely low (<1 μM), we observe that the two-headed nucleotide-free state S7 becomes the major state. This is reasonable because this nucleotide-free state is favorable when short of ATP, which indicates that people should observe again the two-headed state when further decreasing the ATP concentration.

A state detection experiment by Guydosh and Block [23] provided new evidence that single-headed binding dominates kinesin's steps even under small alternating loads (~1.7 pN) when ATP concentration is low (2 μM). For the same loads and ATP concentration, this study predicted that the occurring probability for single-

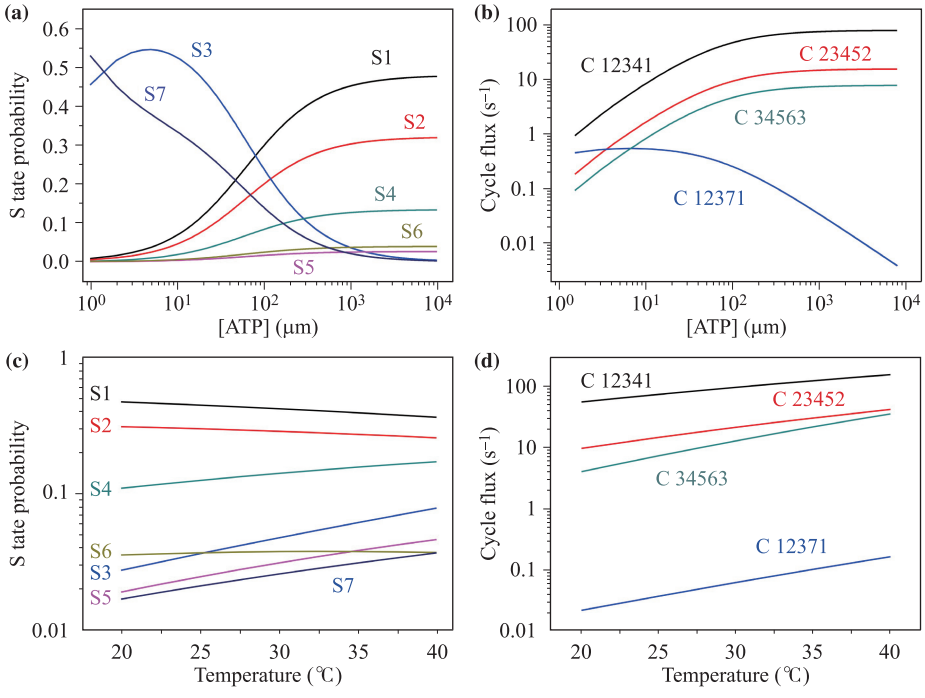

Fig. 3 Occurring probability of states and completion frequencies (fluxes) of cycles in kinesin's steps. A cycle is denoted by a sequence of state numbers in the order by which these states are traversed by the sequential transitions forming the cycle. For example, C12341 marks the cycle S1 → S2 → S3 → S4 → S1. **(a, b)** Room temperature $T_0 = 298$ K. **(c, d)** Load-free condition and [ATP] = 1 mM.

headed binding states [mostly S3, see Fig. 3(a)] is ∼60% vs. 40% for two-headed bindings. A higher percentage of single-headed bindings was estimated by Guydosh and Block [23], probably because the loads, administered in their experiment via a DNA tether attached directly to one head, might destabilize the head-MT binding and reduce the lifetimes of two-headed bindings.

2.5 Consistency with the consensus chemomechanical cycle

Any recurring step of kinesin corresponds to a self-closed cycle of dimer-MT states. Kinesin's underlying kinetic graph dictates what cycles are possible for its steps. The computed frequency for cycle completion (i.e., cycle flux) quantifies the detectability of the chemomechanical cycle during kinesin's steps. We identified kinesin's major chemomechanical cycles in a mathematically rigorous manner, namely, by exhaustively enumerating all possible cycles and ranking them by fluxes [Figs. 3(b, d)]. The cycle ranking shows that a single cycle C12341 (S1 → S2 → S3 → S4 → S1) predominates kinesin's steps in the functionally relevant pre-stall regime [Figs. 3(b, d)]. This cycle indicates that ATP hydrolysis makes the transition S1 → S2, and subsequently the Pi release triggers the head detachment to form the transition S2 → S3. Then, ATP binds to kinesin's MT-bounded head, which induces a neck-linker docking transition (S3 → S4) in the motor domain. The docking transition of the neck-linker rectifies the tethered head toward the next MT binding site (S4 → S1), which completes a full chemomechanical cycle.

For saturated ATP concentrations and zero loads, the flux of this top-ranked cycle is several times higher than that of the second-ranked cycle (C23452). This single-cycle predominance prevails for ATP concentrations down to a few tens of μM [Fig. 3(b)], and over temperature changes from 15 to 40 °C [Fig. 3(d)]. This cycle is the consensus chemomechanical cycle proposed in numerous previous experimental studies [1, 2], which has tight chemomechanical coupling: it achieves a forward step, and consumes one ATP molecule. The predicted dominance of this single cycle is in line with the experimental finding of tight coupling under low loads [42, 43].

2.6 Motility data indicate a systematic velocity-run length scaling

A velocity(ν)-run length(L) scaling of $\nu/L \sim 1/\text{s}$ appears when the temperature-dependent motility data of Nara and Ishiwata [21] are placed in a velocity-run length plot [Fig. 4(c)]. This scaling is meaningful because the data are obtained under vanishing forces and for high ATP concentrations where both velocity and run length saturate toward stable values. When motility data obtained under similar conditions but for kinesin molecules from different species are added to the velocity-run length, these data collapse onto the same $\nu/L \sim 1/\text{s}$ curve. The few deviations are related to discrepant experimental conditions on the same species from different experiments. The result from an experiment [45] on human kinesin falls on the scaling curve, but the result from another [24] lies distant from it. The results from two experiments [19, 44] on rat kinesin both lie away from the scaling curve but on different sides. Altogether, the motility data for different species clearly exhibits the scaling of $\nu/L \sim 1/\text{s}$.

The scaling associated with temperatures is also well reproduced by our theoretical study [see solid line in Fig. 4(c)]. The interspecies scaling is more surprising because previous mutant studies [18] found a decoupling between velocity and run length. Specifically, Thorn, Ubersax, and Vale [18] showed that charged residues engineered into the neck domain drastically changed the run length but barely changed the velocity [Fig. 4(c)]. The interspecies scaling is also different from the $\nu - L$ patterns formed by changing external loads and the ATP concentrations [Figs. 4(a, b)]. The surprising linear scaling might imply that the same chemomechanical cycle dominates across species under functionally relevant conditions.

3 Discussion and conclusions

3.1 ATP gating is indispensable for kinesin's directional and processive steps

The ATP gating is indispensable and largely sufficient for kinesin's processive and directional motility. Cycle C12341, which is predicted to solely dominate kinesin's steps under functionally relevant conditions, relies critically on ATP gating to keep the two heads' catalytic cycles out of phase, particularly at intermediate states S1 and S2. If ATP binding and hydrolysis occur at the front head in either state, concurrent detachments and excessive backward steps would follow to severely reduce both the run length and the plus-end directionality. Hypothetically breaking the ATP gating by allowing ATP binding and hydrolysis leads to a deteriorated agreement with the motility data throughout Figs. 2(a)–(f).

For ADP gating mechanism, a kinetic-graph analysis of the motility data reveal that this mechanism is filtered at least at a low-load regime, which is concerned in present study. In fact, discarding ADP gating by allowing backstepping of S3 will not change the kinesin's motility performance. Thus, the ADP gating seems to be

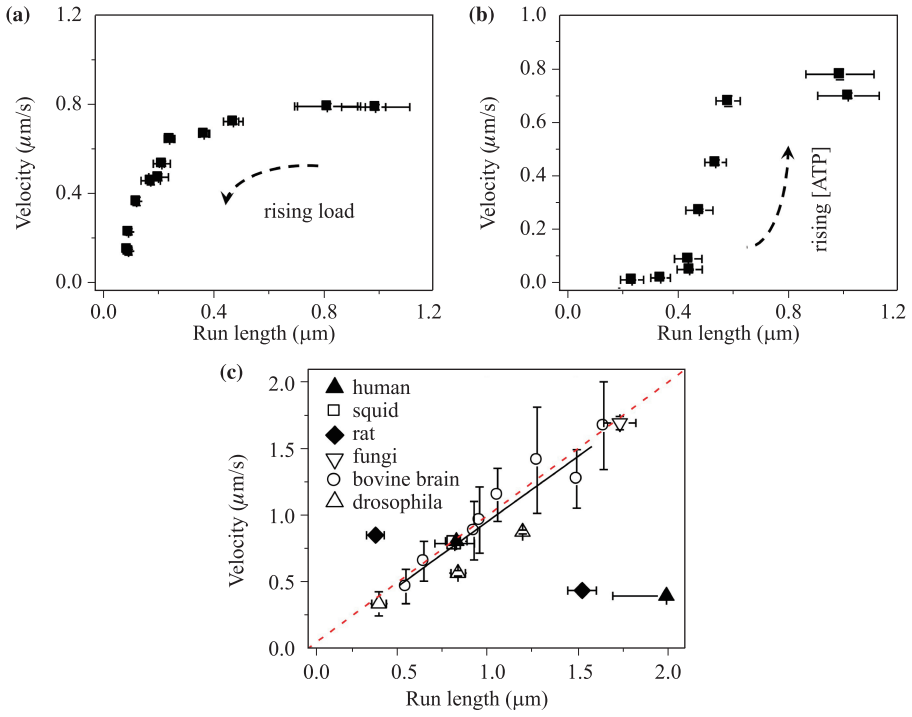

Fig. 4 Velocity-run length ($\nu - L$) correlations for changing loads and ATP concentrations **(a, b)**, and for different species/temperature **(c)**. The symbols are experimental data. They are from Ref. [17] for (a), from Ref. [18] for (b). The data shown in (c) were from Refs. [20, 21] for bovine brain, Refs. [19, 44] for rat, Ref. [45] for fungi, Refs. [14, 17] for squid, Refs. [46–48] for drosophila, Refs. [24, 45] for human. The solid lines in (c) are predictions of this study. The dashed line in (c) indicates the linear scaling $v/L \sim 1/\text{s}$.

a backup mechanism that modulates the kinesin's load-bearing capacity but is not indispensable for either directionality or processivity. By contrast, the ATP gating, on which the major mechanochemical cycles critically rely on, is indispensable and largely sufficient for the kinesin's directionality and high processivity.

With a backup role for ADP gating, kinesin appears dissimilar to actin-based motor myosin V, in which a retarded ADP release at the front head is crucial for the motor's directionality and processivity [49]. In addition to the different positions of gated ADP release, myosin V and kinesin have a reversed order in track-binding affinity for ADP- and ATP-bound motor domains. These differences might underlie the different importance of ADP gating in the two motors. Future comparative study of nucleotide gating in kinesin and myosin will be interesting.

3.2 Linear scaling of velocity-run length

The surprising linear scaling of velocity and run length can be understood by taking a look at the ratio $v/L = p_3^s\gamma_E + (p_4^s + p_5^s)\gamma_T + p_6^s\gamma_D \sim 1/\text{s}$ (see Methods) for the kinetic graph in Fig. 1. As shown in Fig. 3(c), the occurring probability of states maintains an almost constant level as the temperature changes, especially for S6, which possesses the largest derailment rate $\gamma_D = 25\ \text{s}^{-1}$ and contributes most to the ratio, compared with other detachable single-headed states. This robustness of state detectability to temperature changing guarantees the temperature insensitivity of the velocity-run length ratio, which enables the robustness of kinesin functions in a complicated cellular environment. To understand the interspecies scaling, let us write down the ratio of v/L at saturating ATP concentrations (see Methods):

$$v/L = k_{cat}/A = \frac{k_2 k_{-3}[\gamma_T(k_2 + k_{-3} + k_{f2}) + \gamma_D k_2 k_{-3}/k_{-4}]}{k_{f2}(k_2 + k_{-3} + k_{f2})(k_2 + k_{-3}) + k_2 k_{-3}(k_2 + k_{-3} + k_2 k_{-3}/k_{-4})}.$$

Substituting the corresponding rates (see Table 1) into the above expression, one can find the ratio indeed is approximately 1.1/s. On the one hand, this expression of the ratio contains ATP hydrolysis rate k_2, Pi release

Table 1 The values of transition rates used in this study. These kinetic rates are collected under the room temperature condition $T_0 = 298$ K. Other unknown kinetic rates can be inferred by the constraints of thermodynamics consistence under cycle balance condition (see Methods). The temperature-dependence of these kinetic rates is discussed as well (see Methods).

Rate	Meaning	Value	Ref.	Rate	Meaning	Value	Ref.
k_1	ATP binding	3.2 μM^{-1} s^{-1}	[31]	k_{-4}	ADP dissociation	200 s^{-1}	[31]
k_{-1}	ATP dissociation	150 s^{-1}	[31]	k_{f1}	forward diffusive attachment	1 s^{-1}	[32]
k_2	hydrolysis	180 s^{-1}	[31]	k_{f2}	attachment biased by zippering	600 s^{-1}	[32]
k_{-2}	ATP re-synthesis	18 s^{-1}	[31]	γ_E	Derailment from nucleotide-free single-headed binding with MT	0.05 s^{-1}	[32, 33]
k_{-3}	Pi release	300 s^{-1}	[31]	γ_T	Derailment from ATP (or ADP·Pi) retained single-headed binding with MT	0.5 s^{-1}	[32, 33]
k_4	ADP binding	3.2 μM^{-1} s^{-1}	[15]	γ_D	Derailment from ADP retained single-headed binding with MT	25 s^{-1}	[32–34]

ratek_3, and ADP dissociation rate k_{-4}, which all indicate the properties of a nucleotide-associated motor domain. On the other hand, this expression also contains the derailment rates γ_T and γ_D, which indicate the properties of the MT-binding interface of kinesin. Among the interspecies, although different kinesin probably possesses different nucleotide-associated activity (i.e., different k_2, k_3, and k_{-4}), they might also possess different MT-binding interface affinities (i.e., different derailment rates), which can produce a constant velocity-run length ratio. In other words, the interesting linear interspecies scaling implies that there exists a co-evolution between the nucleotide-associated motor domain and the MT-binding interface of kinesin. Nevertheless, the underlying molecular mechanism and functional implications of the unique interspecies scaling deserve future study.

3.3 Onset of new chemomechanical cycles and new detectable states

The present study focuses on the pre-stall regime. Shifts in the cycle flux and detectability of states affected by the ATP concentration and temperature are clearly observed in our theoretical study (see Fig. 3). When the external load becomes significant, more and more new detectable states will emerge, and new chemomechanical cycles will begin. A recent experiment [24] in which both forward and backward consecutive steps were caused by appropriate external loads in a nucleotide-free buffer, signals a new single-head-bounded nucleotide-free state and the onset of a new nucleotide-independent cycle. In a superstall regime where kinesin bears a large load beyond the stall force, Carter and Cross [16] observed consecutive backsteps, which depended on ATP concentrations but not on hydrolysis. This backstepping involving no ATP resynthesis, suggesting that kinesin's backwalking under superstall loads is not a simple reverse of the chemomechanical processes for the forward steps. Some new chemomechanical cycles and new states must emerge to be responsible for the back steps. Our integrative methods enable us to study the onset of new cycles and new states under external loads in the future. This would serve as a useful tool to uncover the working mechanism of kinesin.

3.4 Unified kinetic-graph analysis method

The predictions for cycle fluxes and detectable states came rigorously from the integrative kinetic graph that achieved an overall consistency with existing motility and state detection experiments. This unified kinetic-graph analysis is also a powerful tool for the systematic analysis of kinesin, as demonstrated by the successful identification of the surprisingly simple interspecies scaling. Thus, a unified motility-state analysis based on the kinetic graph is a powerful tool that links motility and state characterization experiments to forge a unified effort for the elucidation of kinesin's underlying kinetic landscape, mechanochemial mechanisms, and systems biology. Graph theory also plays a powerful role in unraveling the underlying nonequilibrium statistical physics of the molecular motor's mechanism, such as supersymmetry, duality [50], and braid group topological phase transition [51]. The method of unified kinetic-graph analysis can be extended to studies of other processive motor proteins such as myosin V and cytoplasmic dynein, where head-head coordination is a common feature.

4 Methods

4.1 Depth-first search algorithm for exhaustive enumeration of cycles

We used an all-cycles enumerating algorithm developed by Tarjan [52]. A graph $G = (V, E)$ consists of a set of

vertices V and links E. A path $(v_1, v_2, \ldots, v_k)$ in a graph is defined as a sequence of links $(v_1, v_2), (v_2, v_3), \ldots, (v_{k-1}, v_k)$ such that the terminal vertex of a link in the sequence is the initial vertex of the next link. A cycle is a path that contains no vertex twice except that its first and last vertices are identical.

The search begins at its arbitrary vertex s, and a path $(s, v_1, v_2, \ldots, v_k)$ is built using a depth-first search procedure. To ensure that each cycle is unique and not simply a circumrotation of a previously found cycle, every vertex v on such a path must satisfy $v \geq s$. As vertices are added to the path, they are marked (to indicate that they are unavailable for extending the current path) and placed onto the stack that records the current path.

We keep extending the path until one of two conditions is met: i) the root s is reached, i.e., a cycle is found, or ii) there is no available vertex to extend the path. Then, we back up one vertex by deleting the top vertex from the stack, and execute another search from the vertex preceding the deleted vertex. If the previous search succeeded in finding a cycle, the deleted vertex should be unmarked as available, because further exploration arriving from another incident link may still lead to a new cycle.

The above process allows us to determine all cycles rooting at s. Continuing the same procedure for all vertices in the graph will enumerate out all cycles. The pseudocode for the cycle search and enumeration is shown below.

Pseudocode for enumerating the cycles:

```
procedure Cycle(v, flag){
flag := false;
path stack := path stack + v;
mark(v) := true;
marked stack := marked stack + v;
for each node w adjacent to v, do {
  if (w < s) {continue;}
  else if (w = s) {
    output cycle from s to v given by path stack;
    flag := true;
  }
  else if (mark(w) = false) {
    g:= Cycle(w, g);
    flag := flag .or. g;
  }
}
if (flag = true) {
    while (top of marked stack ≠ v), do {
      u:= top of marked stack;
      marked stack := marked stack - u;
      mark(u) := false;
    }
    marked stack := marked stack - v;
    mark(v) := false;
}
path stack := path stack - v;
return flag;
}

procedure EnumateCycles() {
for each node s in graph, do {
    Cycle(s, flag);
    while (marked stack not empty), do {
      u:= top of marked stack;
      marked stack := marked stack - u;
      mark(u) := false;
    }
  }
}
```

4.2 Analytical formula for kinesin's motility performance

The kinesin average velocity is a summation over cycles that result in nonzero steps, and each cycle's contribution is proportional to its flux. Organizing the summation according to the flux ranking yields a velocity formula similar to a Taylor expansion. Retaining a limited number of top-ranked cycles and discarding other cycles of diminishing fluxes makes possible a formula that is explicit in its analytical form yet remains a good approximation. We exploited this strategy to obtain analytical formulae for kinesin's velocity (ν) and run length (L) for the physiologically relevant pre-stall regimes. These formulae are in terms of experimentally measurable rates and provide a convenient analytical tool for kinesin study.

At the pre-stall regimes, the cycle ranking [Figs. 3(b, d)] showed that the stepping of kinesin is largely dominated by two forward cycles: C12341 and C23452. Therefore, as a good approximation, we considered only the contributions from these two cycle fluxes to kinesin motility performance:

$$J_{(1,2,3,4,1)} = k_2 k_{-3} k_1 [\mathrm{ATP}] k_{f2} \frac{\det(W[(1,2,3,4);(1,2,3,4)])}{\sum_i \det(W[i;i])}, \tag{2}$$

$$J_{(2,3,4,5,2)} = k_{-3} k_1 [\mathrm{ATP}] k_2 k_{f2} \frac{\det(W[(2,3,4,5);(2,3,4,5)])}{\sum_i \det(W[i;i])}, \tag{3}$$

$$v = L_0 (J_{(1,2,3,4,1)} + J_{(2,3,4,5,2)}), \tag{4}$$

Substitute Eqs. (2) and (3) into Eq. (4), and set the concentration [ADP], [Pi] to be zero such that corresponding transition rates vanish. Then, take the limit of the small rates k_{-2}, k_{f1} approaching zero. Finally, we can obtain the velocity in the Michaelis–Menten form,

$$v = \frac{L_0 \cdot k_{cat}[\mathrm{ATP}]}{[\mathrm{ATP}] + k_{cat}/k_b}, \tag{5}$$

where the catalytic turnover rate (k_{cat}) and the apparent second-order binding rate (k_b) are

$$k_{cat} = \frac{k_2 k_{-3} k_{f2}(k_2 + k_{-3} + k_{f2})}{k_{f2}(k_2 + k_{-3} + k_{f2})(k_2 + k_{-3}) + k_2 k_{-3}(k_2 + k_{-3} + k_2 k_{-3}/k_{-4})}, \tag{6}$$

$$k_b = \frac{k_1 k_2 k_{f2}(k_2 + k_{-3} + k_{f2})}{k_{f2}(k_2 + k_{-3} + k_{f2})(k_2 + k_{-1}) + k_2 k_{-3}(k_2 + k_{-1})}. \tag{7}$$

Using Cramer's rule to get the analytic expressions of $p_3^s, p_4^s, p_5^s, p_6^s$ and substituting them into $L = \frac{v}{\gamma_E p_3^s + \gamma_T(p_4^s + p_5^s) + \gamma_D p_6^s}$, we obtain the mean run length in a similar form

$$L = \frac{L_0 \cdot [\mathrm{ATP}] \cdot A}{[\mathrm{ATP}] + B}, \tag{8}$$

where

$$A = \frac{k_{f2}(k_2 + k_{-3} + k_{f2})}{\gamma_T(k_2 + k_{-3} + k_{f2}) + \gamma_D k_2 k_{-3}/k_{-4}}, \tag{9}$$

$$B = \frac{\gamma_E(k_{-1} + k_2 + k_{f2})(k_{-3} + k_{f2})/k_1}{\gamma_T(k_2 + k_{-3} + k_{f2}) + \gamma_D k_2 k_{-3}/k_{-4}}. \tag{10}$$

At a saturating ATP concentration, $v = L_0 \cdot k_{cat}$ and $L = L_0 \cdot A$, such that the velocity-run length ratio is

$$v/L = k_{cat}/A = \frac{k_2 k_{-3}[\gamma_T(k_2 + k_{-3} + k_{f2}) + \gamma_D k_2 k_{-3}/k_{-4}]}{k_{f2}(k_2 + k_{-3} + k_{f2})(k_2 + k_{-3}) + k_2 k_{-3}(k_2 + k_{-3} + k_2 k_{-3}/k_{-4})}. \tag{11}$$

4.3 Thermodynamics consistency of rates using cycle balance condition

When external force is negligible, as in our case, the rates along any cycle $(i_1, i_2, \ldots, i_m, i_1)$ are required by thermodynamics consistency to satisfy the cycle balance condition [30, 53]: $\frac{\omega_{i_1 i_m} \cdots \omega_{i_3 i_2} \omega_{i_2 i_1}}{\omega_{i_1 i_2} \omega_{i_2 i_3} \cdots \omega_{i_m i_1}} = \mathrm{e}^{\frac{\Delta\mu}{k_B T}}$, where $\Delta\mu$ is the free energy utilized in cycle $(i_1, i_2, \ldots, i_m, i_1)$. For cycles without ATP hydrolysis, $\Delta\mu = 0$; for cycles that involve ATP hydrolysis, $\Delta\mu = k_B T \ln\left(\frac{K_{\mathrm{eq}}[\mathrm{ATP}]}{[\mathrm{ADP}][P]}\right)$, where $K_{\mathrm{eq}} = 4.9 \times 10^{11}$ μM. In other words, for the ATP hydrolysis cycle, $\frac{\omega_{i_1 i_m} \cdots \omega_{i_3 i_2} \omega_{i_2 i_1}}{\omega_{i_1 i_2} \omega_{i_2 i_3} \cdots \omega_{i_m i_1}} = \frac{K_{\mathrm{eq}}[\mathrm{ATP}]}{[\mathrm{ADP}][\mathrm{P}]}$; otherwise, $\frac{\omega_{i_1 i_m} \cdots \omega_{i_3 i_2} \omega_{i_2 i_1}}{\omega_{i_1 i_2} \omega_{i_2 i_3} \cdots \omega_{i_m i_1}} = 1$.

For C34563, we have the constraint $\frac{k_1 \cdot k_2 \cdot k'_{-3} \cdot k_{-4}}{k_{-1} \cdot k_{-2} \cdot k'_3 \cdot k_4} = K_{\mathrm{eq}}$, where k'_{-3} and k'_3 denote the Pi release and rebinding rates for single-headed kinesin. If $k'_{-3} = k_{-3}$ is assumed, from the constraint, we obtain an extremely small value $k'_3 \approx 8.16 \times 10^{-9}$ μM^{-1} s^{-1}.

For C12341 and C12371, we have $\frac{k_1 \cdot k_2 \cdot k_{-3} \cdot k_{f2}}{k_{-1} \cdot k_{-2} \cdot k_3 \cdot k_{-f2}} = K_{\mathrm{eq}}$ and $\frac{k_1 \cdot k_2 \cdot k_{-3} \cdot k_{f1}}{k_{-1} \cdot k_{-2} \cdot k_3 \cdot k_{-f1}} = K_{\mathrm{eq}}$, which indicates that $k_3 k_{-f2} = 7.8 \times 10^{-8}$ μM^{-2} s^{-2} and $k_3 k_{-f2} = 1.3 \times 10^{-10}$ μM^{-2} s^{-2}. All these results indicate that the rebinding rates of ADP and Pi usually are very small. In fact, the ATP hydrolysis cycle is an energetically steep downhill process and possesses high irreversibility, which usually makes the rates along the reverse direction significantly smaller. In our calculations, since we set [ADP] = 0 and [Pi] = 0, the corresponding nucleotide-rebinding processes are ignored. Even when we consider finite values of these rates, we checked that these negligible processes will not affect our results at all.

4.4 Temperature dependence of kinetic rates

The temperature dependence of enzymatic activity and diffusive head attachment were considered by assuming an Arrhenius form for the respective rates. The activation energies for ATP dissociation, hydrolysis, and Pi release were taken as 50 kJ/mol from the experiments of Ishiwata *et al.* [20, 21]. The experiments indicated a higher activation energy for ADP release, which was assumed as 80 kJ/mol here. The activation energy for diffusive head attachment was computed previously [27] and is 20 kJ/mol and 40 kJ/mol for zipper-biased attachment (k_{f2}) and diffusive attachment (k_{f1}), respectively.

The rates given in Table I were under room temperature $T_0 = 298$ K (note: 1 kJ/mol $= 0.4034 k_B T_0$). The temperature dependence of the head detachment rates were suggested to be small (or possibly of endothermic nature) by the experiments of Ishiwata *et al.* [20, 21], and was ignored here as an approximation. The detailed temperature-dependences of other kinetic rates are given as

$$k_{f1}(T) = 1\ \mathrm{s}^{-1} \cdot \exp\left(-\frac{\Delta E_{f1}}{k_B T_0} \cdot \frac{T_0 - T}{T}\right), \quad k_{f2}(T) = 600\ \mathrm{s}^{-1} \cdot \exp\left(-\frac{\Delta E_{f2}}{k_B T_0} \cdot \frac{T_0 - T}{T}\right), \tag{12}$$

$$k_{-1}(T) = 150\ \mathrm{s}^{-1} \cdot \exp\left(-\frac{\Delta E}{k_B T_0} \cdot \frac{T_0 - T}{T}\right), \quad k_2(T) = 180\ \mathrm{s}^{-1} \cdot \exp\left(-\frac{\Delta E}{k_B T_0} \cdot \frac{T_0 - T}{T}\right), \tag{13}$$

$$k_{-2}(T) = 18\ \mathrm{s}^{-1} \cdot \exp\left(-\frac{\Delta E}{k_B T_0} \cdot \frac{T_0 - T}{T}\right), \quad k_{-3}(T) = 300\ \mathrm{s}^{-1} \cdot \exp\left(-\frac{\Delta E}{k_B T_0} \cdot \frac{T_0 - T}{T}\right), \tag{14}$$

$$k_{-4}(T) = 200\ \mathrm{s}^{-1} \cdot \exp\left(-\frac{\Delta E_{-4}}{k_B T_0} \cdot \frac{T_0 - T}{T}\right), \tag{15}$$

where $\Delta E \sim 20 k_B T_0$, $\Delta E_{f1} = 15 k_B T_0$, $\Delta E_{f2} = 9 k_B T_0$, $\Delta E_{-4} = 33 k_B T_0$.

Acknowledgements Jie Ren thanks Prof. Zhisong Wang from NUS for his generous guidance and improvements on this project. This work was partly supported by the National Youth 1000 Talents Program in China, and the startup grant (No. 205020516074) at Tongji University.

References

1. R. D. Vale and R. A. Milligan, The way things move: Looking under the hood of molecular motor proteins, *Science* 288(5463), 88 (2000)
2. S. M. Block, Kinesin motor mechanics: Binding, stepping, tracking, gating, and limping, *Biophys. J.* 92(9), 2986 (2007)
3. A. Gennerich and R. D. Vale, Walking the walk: How kinesin and dynein coordinate their steps, *Curr. Opin. Cell Biol.* 21(1), 59 (2009)
4. S. S. Rosenfeld, P. M. Fordyce, G. M. Jefferson, P. H. King, and S. M. Block, Stepping and Stretching: How kinesin uses internal strain to walk processively, *J. Biol. Chem.* 278(20), 18550 (2003)
5. L. M. Klumpp, A. Hoenger, and S. P. Gilbert, Kinesin's second step, *Proc. Natl. Acad. Sci. USA* 101(10), 3444 (2004)
6. N. R. Guydosh and S. M. Block, Backsteps induced by nucleotide analogs suggest the front head of kinesin is gated by strain, *Proc. Natl. Acad. Sci. USA* 103(21), 8054 (2006)
7. D. D. Hackney, Evidence for alternating head catalysis by kinesin during microtubule-stimulated ATP hydrolysis, *Proc. Natl. Acad. Sci. USA* 91(15), 6865 (1994)
8. Y. Z. Ma and E. W. Taylor, Interacting head mechanism of microtubule-kinesin ATPase, *J. Biol. Chem.* 272(2), 724 (1997)
9. S. Uemura and S. Ishiwata, Loading direction regulates the affinity of ADP for kinesin, *Nat. Struct. Biol.* 10(4), 308 (2003)
10. A. B. Asenjo, N. Krohn, and H. Sosa, Configuration of the two kinesin motor domains during ATP hydrolysis, *Nat. Struct. Biol.* 10(10), 836 (2003)
11. A. Yildiz, M. Tomishige, R. D. Vale, and P. R. Selvin, Kinesin walks hand-over-hand, *Science* 303(5658), 676 (2004)
12. T. Mori, R. D. Vale, and M. Tomishige, How kinesin waits between steps, *Nature* 450(7170), 750 (2007)
13. A. B. Asenjo and H. Sosa, A mobile kinesin-head intermediate during the ATP-waiting state, *Proc. Natl. Acad. Sci. USA* 106(14), 5657 (2009)
14. K. Visscher, M. J. Schnitzer, and S. M. Block, Single kinesin molecules studied with a molecular force clamp, *Nature* 400(6740), 184 (1999)
15. W. R. Schief, R. H. Clark, A. H. Crevenna, and J. Howard, Inhibition of kinesin motility by ADP and phosphate supports a hand-over-hand mechanism, *Proc. Natl. Acad. Sci. USA* 101(5), 1183 (2004)
16. N. J. Carter and R. A. Cross, Mechanics of the kinesin step, *Nature* 435(7040), 308 (2005)
17. M. J. Schnitzer, K. Visscher, and S. M. Block, Force production by single kinesin motors, *Nat. Cell Biol.* 2(10), 718 (2000)
18. K. S. Thorn, J. A. Ubersax, and R. D. Vale, Engineering the processive run length of the kinesin motor, *J. Cell Biol.* 151(5), 1093 (2000)
19. J. Yajima, M. C. Alonso, R. A. Cross, and Y. Y. Toyoshima, Direct long-term observation of kinesin processivity at low load, *Curr. Biol.* 12(4), 301 (2002)
20. K. Kawaguchi and S. Ishiwata, Temperature dependence of force, velocity, and processivity of single kinesin molecules, *Biochem. Biophys. Res. Commun.* 272(3), 895 (2000)

21. I. Nara and S. Ishiwata, Processivity of kinesin motility is enhanced on increasing temperature, *Biophysics* 2, 13 (2006)
22. S. Uemura, K. Kawaguchi, J. Yajima, M. Edamatsu, Y. Y. Toyoshima, and S. Ishiwata, Kinesin-microtubule binding depends on both nucleotide state and loading direction, *Proc. Natl. Acad. Sci. USA* 99(9), 5977 (2002)
23. N. R. Guydosh and S. M. Block, Direct observation of the binding state of the kinesin head to the microtubule, *Nature* 461(7260), 125 (2009)
24. A. Yildiz, M. Tomishige, A. Gennerich, and R. D. Vale, Intramolecular strain coordinates kinesin stepping behavior along microtubules, *Cell* 134(6), 1030 (2008)
25. Q. Shao and Y. Q. Gao, On the hand-over-hand mechanism of kinesin, *Proc. Natl. Acad. Sci. USA* 103(21), 8072 (2006)
26. W. W. Zheng, D. Fan, M. Feng, and Z. S. Wang, Load-resisting capacity of kinesin, *Phys. Biol.* 6(3), 036002 (2009)
27. Z. S. Wang, M. Feng, W. W. Zheng, and D. G. Fan, Kinesin is an evolutionarily fine-tuned molecular ratchet-and-pawl device of decisively locked directionality, *Biophys. J.* 93(10), 3363 (2007)
28. C. Hyeon and J. N. Onuchic, Internal strain regulates the nucleotide binding site of the kinesin leading head, *Proc. Natl. Acad. Sci. USA* 104(7), 2175 (2007)
29. Y. Okada and N. Hirokawa, Mechanism of the single-headed processivity: Diffusional anchoring between the K-loop of kinesin and the C terminus of tubulin, *Proc. Natl. Acad. Sci. USA* 97(2), 640 (2000)
30. S. Liepelt and R. Lipowsky, Kinesin's network of chemomechanical motor cycles, *Phys. Rev. Lett.* 98(25), 258102 (2007)
31. R. A. Cross, The kinetic mechanism of kinesin, *Trends Biochem. Sci.* 29(6), 301 (2004) (and references therein)
32. D. G. Fan, W. W. Zheng, R. Hou, F. Li, and Z. S. Wang, Modelling motility of the kinesin dimer from molecular properties of individual monomers, *Biochemistry* 47(16), 4733 (2008)
33. W. O. Hancock and J. Howard, Kinesin's processivity results from mechanical and chemical coordination between the ATP hydrolysis cycles of the two motor domains, *Proc. Natl. Acad. Sci. USA* 96(23), 13147 (1999)
34. S. D. Auerbach and K. A. Johnson, Alternating site ATPase pathway of rat conventional kinesin, *J. Biol. Chem.* 280(44), 37048 (2005)
35. T. L. Hill, Studies in irreversible thermodynamics (IV): Diagrammatic representation of steady-state fluxes for unimolecular systems, *J. Theor. Biol.* 10(3), 442 (1966)
36. T. L. Hill and Y. D. Chen, Stochatics of cycle completions (fluxes) in biochemical kinetic diagram, *Proc. Natl. Acad. Sci. USA* 72(4), 1291 (1975)
37. H. H. Kohler and E. Vollmerhaus, The frequency of cyclic processes in biological multistate systems, *J. Math. Biol.* 9(3), 275 (1980)
38. W. T. Tutter, Graph Theory, Cambridge: Cambridge University Press, 2001
39. E. L. King and C. Altman, A schematic method of deriving the rate laws for enzyme-catalyzed reactions, *J. Phys. Chem.* 60(10), 1375 (1956)
40. S. M. Block, C. L. Asbury, J. W. Shaevitz, and M. J. Lang, Probing the kinesin reaction cycle with a 2D optical force clamp, *Proc. Natl. Acad. Sci. USA* 100(5), 2351 (2003)
41. S. Rice, A. W. Lin, D. Safer, C. L. Hart, N. Naber, B. O. Carragher, S. M. Cain, E. Pechatnikova, E. M. Wilson-Kubalek, M. Whittaker, E. Pate, R. Cooke, E. W. Taylor, R. A. Milligan, and R. D. Vale, A structural change in the kinesin motor protein that drives motility, *Nature* 402(6763), 778 (1999)
42. W. Hua, E. C. Young, M. L. Fleming, and J. Gelles, Coupling of kinesin steps to ATP hydrolysis, *Nature* 388(6640), 390 (1997)
43. M. J. Schnitzer and S. M. Block, Kinesin hydrolyses one ATP per 8-nm step, *Nature* 388(6640), 386 (1997)
44. A. Seitz, H. Kojima, K. Oiwa, E. M. Mandelkow, Y. H. Song, and E. Mandelkow, Single-molecule investigation of the interference between kinesin, tau and MAP2c, *EMBO J.* 21(18), 4896 (2002)
45. S. Lakämper, A. Kallipolitou, G. Woehlke, M. Schliwa, and E. Meyhofer, Single fungal kinesin motor molecules move processively along microtubules, *Biophys. J.* 84(3), 1833 (2003)
46. R. D. Vale, T. Funatsu, D. W. Pierce, L. Romberg, Y. Harada, and T. Yanagida, Direct observation of single kinesin molecules moving along microtubules, *Nature* 380(6573), 451 (1996)
47. D. L. Coy, M. Wagenbach, and J. Howard, Kinesin takes one 8-nm step for each ATP that it hydrolyzes, *J. Biol. Chem.* 274(6), 3667 (1999)
48. S. Courty, C. Luccardini, Y. Bellaiche, G. Cappello, and M. Dahan, Tracking individual kinesin motors in living cells using single quantum-dot imaging, *Nano Lett.* 6(7), 1491 (2006)
49. D. Vale, Myosin V motor proteins, *J. Cell Biol.* 163, 445 (2003)
50. J. Ren, V. Y. Chernyak, and N. A. Sinitsyn, Duality and fluctuation relations for statistics of currents on cyclic graphs, *J. Stat. Mech.: Theo. Exp.* 05, 05011 (2011)
51. J. Ren and N. A. Sinitsyn, Braid group and topological phase transitions in nonequilibrium stochastic dynamics, *Phys. Rev. E* 87(5), 050101 (2013) (R)
52. R. Tarjan, Enumeration of the elementary circuits of a directed graph, *SIAM J. Comput.* 2(3), 211 (1973)
53. L. Onsager and S. Machlup, Fluctuations and irreversible processes, *Phys. Rev.* 91(6), 1505 (1953)